High resolution crystal structure of substrate-free human neprilysin

Stephen Moss, Vasanta Subramanian, K. Ravi Acharya*

Department of Biology and Biochemistry, Claverton Down, University of Bath, Bath BA2 7AY, UK

*Corresponding author at: Department of Biology and Biochemistry, University of Bath, Claverton Down, Bath BA2 7AY, UK.
E-mail: bsskra@bath.ac.uk (K. Ravi Acharya)

Keywords: Neprilysin; Zinc metalloprotease; Protein structure; Crystallography; Substrate-free

Abstract

Neprilysin is a transmembrane M13 zinc metalloprotease responsible for the degradation of several biologically active peptides including insulin, enkephalin, substance P, bradykinin, endothelin-1, neurotensin and amyloid-β. The protein has received attention for its role in modulating blood pressure responses with its inhibition producing an antihypertensive response. To date, several inhibitor bound crystal structures of the human neprilysin extracellular domain have been determined, but, a structure free of bound inhibitor or substrate has yet to be reported. Here, we report the first crystal structure free of substrate or inhibitor for the extracellular catalytic domain of human neprilysin at 1.9 Å resolution. This structure will provide a reference point for comparisons to future inhibitor or substrate bound structures. The neprilysin structure also reveals that a closed protein conformation can be adopted in protein crystals absent of bound substrate or inhibitor.

1. Introduction

Neprilysin (NEP, EC 3.4.24.11), also known as neutral endopeptidase, neuropeptidase, CD10 and enkephalin, is a transmembrane protease that belongs to the M13 family of zinc metalloproteases. NEP can digest a broad range of peptide substrates including insulin, enkephalin, substance P, bradykinin, endothelin-1, neurotensin and amyloid-β (Kerr *et al*., 1974; Skidgel *et al*., 1984; Howell *et al*., 1995). In addition to the broad substrate specificity, NEP can cleave each substrate at a number of locations but exhibits a preference for the amino side of hydrophobic residues (Hersh *et al*., 1986).

NEP is located at the plasma membrane and consist of three domains. The short intracellular and transmembrane domains are 27 and 23 residues in length and the third larger extracellular catalytic domain which is 699 residues in length. The extracellular domain contains a large central cavity where the conserved zinc binding motif HEXXH is located. The two histidine residues are responsible for the coordination of the zinc ion, while the glutamate is directly involved in catalysis. This conserved region has been targeted for inhibition to produce an antihypertensive response. To date eight inhibitor bound structures of the human NEP extracellular domain are available in the Protein Data Bank (Oefner *et al*., 2000; Oefner *et al*., 2004; Sahli *et al*., 2005; Oefner *et al*., 2007; Glossop *et al*., 2011; Schiering *et al*., 2016) but a structure free of bound inhibitor or substrate has yet to be reported. Here, we report the first crystal structure of the substrate-free extracellular domain of human NEP.

2. Materials and methods

2.1 Expression and purification

All reagents for expression and purification were sourced from Sigma-Aldrich or Fisher Scientific unless otherwise specified.

A clone of *Pichia pastoris* GS115 expressing the extracellular catalytic domain of human NEP was purchased from Invitrogen. The clone contained human NEP (Tyr51-Trp749) integrated into the *P. pastoris* genome. The cytoplasmic (Gly1-Glu27) and

transmembrane (Ile28-Ala50) domains of NEP were absent in the construct to increase the probability of protein crystallisation. The protein of interest was expressed with an N-terminal 6x histidine tag and a secretion peptide sequence.

Expression of the *P. pastoris* clone was completed in accordance with the Invitrogen manual for recombinant protein expression. A glycerol stock of the *P. pastoris* clone was used to inoculate a starter culture containing 25ml of BMGY (1% Yeast extract, 2% Peptone, 22.968 g L^{-1} K_2HPO_4, 118.048 g L^{-1} KH_2PO_4 pH 6.0, 1.34% Yeast nitrogen base, $4x10^{-5}$% Biotin and 1% Glycerol) in a 250 mL baffled flask. The starter culture was incubated overnight at 30ºC. 10 mL of the overnight culture was used to inoculate an expression culture in 2 L baffled flasks containing 250 mL BMGY. The expression culture was incubated at 30ºC for 24 hours.

After 24 hours the expression culture was harvested at 6000 RCF for 20 minutes at 19ºC. The supernatant was discarded, and the cell pellet was re-suspended in 250 mL of BMMY (1% Yeast extract, 2% Peptone, 22.968 g L^{-1} K_2HPO_4, 118.048 g L^{-1} KH_2PO_4 pH 6.0, 1.34% Yeast nitrogen base, $4x10^{-5}$% Biotin and 0.5% Methanol) for induction. Re-suspended cells were transferred to a new 2 L baffled flask. The culture was incubated for 72 hours at 30ºC. 5 mL of 50% methanol was added to the culture 24 and 48 hours.

After 72 hours of induction the culture was harvested at 6000 RCF for 20 minutes at 19ºC. The supernatant was collected and the cell pellet was discarded. Tris and NaCl were added to the supernatant to give final concentrations of 25 mM Tris and 150 mM NaCl. Following the addition of Tris and NaCl the supernatant showed some precipitation which was removed through a 0.22 µm filter (Millipore).

The *P. pastoris* culture supernatant was loaded onto a 5 mL HisTrap affinity column (GE Healthcare Life Sciences) at 2 mL min^{-1} pre-equilibrated with Buffer A (25 mM Tris, 150 mM NaCl, 2 mM $MgCl_2$ pH 7.5). Following loading, the column was washed with 2% Buffer B (25 mM Tris, 150 mM NaCl, 2 mM $MgCl_2$ and 500 mM Imidazole pH 7.5) until the UV trace returned to baseline. Bound NEP was eluted using a gradient of Buffer B between 2-100%. 2 mL fractions were collected and analysed using SDS-PAGE with a 10%

acrylamide gel to confirm the presence of protein.

Fractions containing protein were concentrated to a volume under 5 mL in a centrifuge at 4000 RCF. For concentration a centrifuge filter unit with a 30 kDa molecule weight cut off (Millipore) was used. The concentrated protein containing sample was then loaded at 5 mL min^{-1} onto a HiPrep 26/10 Desalting column (GE Healthcare Life Sciences) pre-equilibrated with Buffer A. Eluted protein containing fractions were kept at 4°C for short term storage or -20°C for longer term storage.

2.2 Enzymatic assay

The enzymatic activity of NEP was assayed by measuring cleavage of the fluorogenic peptide Mca-RPPGFSAFK-(Dnp) (Enzo Life Sciences). A stock solution of 1 mM Mca-RPPGFSAFK(Dnp) dissolved in 100% DMSO was stored at -20°C. Dilutions of this stock where made using purification Buffer A. Enzymatic assays were conducted using 50 µL of 20 µM Mca-RPPGFSAFK-(Dnp) and 50 µL of 8 nM purified NEP. 50 µL of 8 nM bovine serum albumin (BSA) was used as a negative control. Solutions were manually added to a black 96 well microplate (Greiner Bio-One).

Fluorescence activity assays were performed using a CLARIOstar high-performance microplate reader (BMG LABTECK). Excitation was achieved at 328 nm and emission was detected at 393 nm. Readings were taken in triplicate at 15 second intervals for a length of 45 minutes.

2.3 Crystallisation

Protein crystallisation was performed with NEP (8 mg/mL) mixed 1:1 with crystallisation buffer 0.2 M KNO_3 and 20% (w/v) PEG3350 (Molecular Dimensions, England). The mixed solution was manually dispensed into 24-well plates (Molecular Dimensions, England) for crystallisation experiments using hanging drop vapour diffusion. Plates were stored at 18°C and crystals formed within a month. Crystals used for data collection were mounted in a loop and flash-cooled for storage in liquid nitrogen without cryoprotectant.

2.4 Data collection, structure determination and refinement

X-ray diffraction data were collected at the i03 beamline in Diamond Light Source (Didcot, Oxford) at a wavelength of 0.976 Å (12.7 keV) with an oscillation range of 0.1^{o} using a Pilatus3 6M detector.

Raw X-ray diffraction data were indexed and integrated using DIALS (Waterman *et al*., 2016). Data were then scaled and merged using AIMLESS within the CCP4 suite (Evans *et al*., 2013; Winn *et al*., 2011). A resolution cut off of 1.9 Å was applied based on statistics generated from AIMLESS (Evans *et al*., 2013).

PHASER (McCoy *et al*., 2007) was used to perform molecular replacement using structure 5JMY (Schiering *et al.,* 2016) on the merged and scaled data from AIMLESS. A single structural solution was provided with a TFZ score of 14.18. After PHASER the structure was refined using REFMAC5 (Murshudov *et al*., 2011). PHENIX was used towards the end of refinement for its superior handling of protein glycosylation (Adams *et al*., 2010). Visualisation and model building were performed using COOT (Emsley *et al*., 2010).

Programs MolProbity (Chen *et al*., 2010) and PDB validation (Berman *et al*., 2003) were used to assess any steric and geometry outliers within the modelled structure. The coordination of the active site zinc ion was assessed using the CheckMyMetal server (Zheng *et al*., 2017) and a composite omit map was generated using Phenix (Terwilliger *et al*., 2008) to provide a bias free map of the active site. Images were created using either PyMOL (Schrödinger, LLC, 2015) or CCP4mg (McNicholas *et al*., 2011) and APBS was used for determination of protein cavity electrostatic potential (Baker *et al*., 2001). RMSD values for main chain superpositions were calculated using LSQ in COOT (Emsley *et al*., 2010) and cavity volumes were calculated using CASTp (Binkowski *et al*., 2003).

The final refined structure had R_{work} and R_{free} of 18.99% and 23.54% respectively and was deposited with the Protein Data Bank under code 6GID (Table 1).

3. Results and discussion

Here we report the first substrate-free crystal structure for the extracellular catalytic domain

of human NEP (Gly54-Trp749). The structure was determined in the trigonal space group $P3_221$ with a single molecule in the asymmetric unit to a resolution of 1.9 Å. The protein used for this structural study was expressed and purified in *P. pastoris* and has been shown to be catalytically active (Figure 1).

The reported structure was refined to give final R_{work} and R_{free} values of 18.99% and 23.54% respectively. Overall, 98% of residues are within the preferred region of the Ramachandran plot with 2% allowed and no outliers. The details of data collection and refinement statistics are presented in Table 1.

3.1 General features

The NEP extracellular domain is ellipsoid in shape with a long and short axis of 86 Å and 60 Å respectively. The secondary structure of NEP is mainly alpha helical in nature and can be further separated into two large lobe-like subdomains connected by a smaller linker region. The linker region is formed of four alpha helical segments distributed non-consecutively in the protein sequence (Figure 2). Subdomain 1 consists of N-terminal residues while subdomain 2 consists of C-terminal residues. Together, subdomains 1 and 2 enclose a large central cavity.

Four sites of *N*-linked glycosylation have been confirmed at positions N144, N284 and N324 in subdomain 2 and position N627 in subdomain 1. Electron density allowed a single *N*-acetylglucosamine residue to be modelled at each of these sites.

The catalytic site of NEP, located within the cavity surface of subdomain 1, is based around a zinc ion and conserved active site motif HEXXH. The zinc ion is coordinated by conserved residues H583 (2.02 Å) and H587 (2.10 Å) and additional coordination is provided by E646 (1.93 Å). The third conserved residue, E584, is involved in the catalytic mechanism and adopts a position above the zinc ion completing coordination sphere.

The coordinated zinc ion and surrounding residues creates a small binding pocket with subsites S1, S1' and S2' (Figure 3). Inhibitors designed for NEP have revealed characteristics about the subsites. The S1 site has low impact on the overall affinity for

binding and displays relaxed specificity (Oefner *et al*., 2000). S1' subsite forms a hydrophobic pocket that exhibits specificity for large hydrophobic and aromatic side chains (Tiraboschi *et al*., 1999). This accounts for the preference for NEP to cleavage sites at the amino side of hydrophobic residues. The S2' subsite displays relaxed specificity and can accommodate bulky side chains (Dion *et al*., 1997).

3.2 Modelling active site density

In addition to residues H583, H587 and E646, a ligand is required to create an acceptable coordination sphere for the catalytic zinc ion. In the structure reported here, this is provided by a phosphate ion (2.07 Å and 2.36 Å) carried through from the *P. pastoris* expression growth media. The final refined structure shows the modelled phosphate ion has a good fit to the electron density (Figure 4A). A composite omit map was used to generate bias-free electron density for the region surrounding the catalytic zinc ion (Figure 4B). The omit map supported the placement of the phosphate ion, with good density present above the zinc ion. The full coordination sphere was evaluated using the CheckMyMetal web server (Zheng *et al*., 2017) to confirm the acceptable coordination interactions were modelled.

The presence of a ligand coordinating the catalytic zinc ion has been reported in other native zinc metalloprotease crystal structures that share the HEXXH motif. In angiotensin-converting enzyme (ACE, 1O8A) an acetate is responsible for coordinating the zinc atom (Natesh *et al*., 2003). Other structures including insulin-degrading enzyme (IDE, 2JG4) (Im *et al*., 2007) and thermolysin (1TLX and 2TLX) (English *et al*., 1999), have water molecules coordinating the zinc ion. However, in these structures the water molecule does not completely account for the electron density above the zinc ion and the coordination distances between water molecule and the zinc ion are greater than acceptable lengths (Zheng *et al*., 2017).

It is clear that the molecule responsible for the coordination of the catalytic zinc ion has an area of density that is difficult to model with certainty in native zinc metalloprotease structures. It is likely that a range of ligands or water molecules are responsible for coordinating the zinc ion across the different protein molecules present within the protein

crystal. As a result, the density describes an average of these ligands and water molecules. In the structure reported here, a phosphate ion has been modelled to coordinate the zinc ion based on the evidence present above.

The structure reported here contains additional weaker density in the S1' and S2' subsites. That weaker density has been modelled as a polyethylene glycol fragment (PEG) acquired from the crystallisation buffer. Occupancy of the PEG fragment was refined using Phenix to 0.95. The fragment has several favourable contacts to the phosphate ion but has limited interactions to active site residues with no contacts closer than 3.15 Å in length.

The native ACE, IDE and thermolysin structures also exhibit additional weak density in the active site. It is likely that a range of small molecules present in the crystallisation buffers show affinity for the binding site accounting for weak density in the region. Due to the presence of a PEG molecule and phosphate ion we describe this structure as substrate-free opposed to native.

3.3 Active site flexibility

To date, eight inhibitor bound crystal structures of NEP extracellular domain are currently available in the Protein Data Bank. These structures were superimposed onto the substrate-free NEP structure and active site residues were visually inspected for conformational changes. Two inhibitor bound structures were selected to accurately describe all conformational changes that were present across the eight available structures. These two structures are compared to substrate-free NEP below.

First, the substrate-free crystal structure is compared to crystal structure 5JMY (Schiering *et al.,* 2016) which contains inhibitor LBQ657. Conformational changes in residues F106 and W693 can be seen between our substrate-free structure and 5JMY (Figure 5A). W693 displays a large shift that increases the volume of the S1' pocket and allows the biphenyl group of LBQ657 to occupy the site. The shift in W693 causes rotation in F106 altering the S2' subsite. The second comparison is to crystal structure 1DMT (Oefner *et al.,* 2000) which contains inhibitor phosphoramidon. Conformational changes in R110 form the interface of the S2’ subsite and accommodate for the bulky side chain of

phosphoramidon (Figure 5B).

The flexibility in residues listed above helps explain how NEP can accommodate a number of different peptide substrates at different locations with variability in the specific amino acid that interacts with the cleavage site. W693, F106 and R110 are the only active site amino acids that show significant motions when compared to the eight published inhibitor bound crystal structures.

3.4 Conformational flexibility

The crystal structure reported here for the NEP extracellular domain is in a closed conformation. Two small solvent accessible entrances to the large cavity are located at the front and rear of the protein measuring approximately 8 Å and 6 Å at their narrowest points (Figure 7A). These entrances are too small for the entry of substrate or inhibitor indicating NEP must undergo conformational changes to adopt an open conformation.

Published inhibitor bound structures all report NEP in closed conformations. Superpositions of these structures with substrate-free NEP (Figure 6), and RMSD values calculated for the superpositions (Table 2), indicate the close conformational similarity. This reveals binding of substrate or inhibitor is not required to stabilise the closed conformation in the NEP crystal structure. It is unclear if the protein only opens when interacting with substrate or whether the closed conformation is a result of the protein existing in a crystal structure.

In a closed conformation NEP's large central cavity has an approximate volume of 5000 $Å^3$ which is a smaller volume than many of the peptides it is responsible for cleaving (Malito *et al*., 2008). Previous studies have revealed amyloid-β, a substrate of NEP, is cleaved at a number of locations within the centre of the polypeptide chain (Sexton *et al*., 2012; Webster *et al*., 2014). Cleavage in this manner is a characteristic feature seen in other zinc metalloproteases including insulin degrading enzyme (IDE) which has a similar the two lobe-like domain structure with large central cavities.

In order for substrate cleavage to occur, it is likely that large movements in the

subdomains are required for substrate access into the active site. Structures of IDE have revealed that a separation of the two lobe-like domains allows entry of substrate before a closed conformation is adopted completely engulfing the substrate into the central cavity (McCord *et al*., 2013). Given the smaller size of the NEP cavity it is unlikely that the protein completely engulfs its substrate, but it is clear that motion is required for access to the active site. The exact mechanism will remain elusive until peptide bound structures of NEP are determined.

The electrostatic surface charge of the cavity has been analysed using APBS (Figure 7B). A striking electrostatic difference between the top and bottom surfaces of the cavity is present. The top surface, contributed by subdomain 2, displays a large area of positive electrostatic potential. The opposite is observed for the bottom surface, contributed by subdomain 1, where a large negative electrostatic potential is present in and in proximity to the catalytic site. It is also observed that the front entrance to the cavity possesses a strong negative electrostatic potential, while the rear entrance possesses a strong positive electrostatic potential. These electrostatic features may be critical for guidance of substrate to the active site and important for substrate binding.

4. Conclusion

In this report we have presented a substrate-free crystal structure for the extracellular domain of human NEP. The active site of this structure has been compared to other available inhibitor bound structures revealing flexibility in active site residues W693, F106 and R110. Flexibility in these residues is critical for allowing the active site to accommodate a variety of substrates binding at a range of positions. Additionally, we also note the central cavity of NEP has striking electrostatic potential differences between the top and bottom side. The function of these differences is unknown but are likely involved in substrate interaction.

The crystal structure of substrate-free NEP reveals that a closed protein conformation can be retained in the absence of bound substrate or inhibitor. The mechanism for

substrate entrance into the active site remains unclear, but clues provided by IDE suggest large domain shifts may be required for substrate entry. The structure reported here provides a key reference point for any future structural studies investigating substrate binding and conformational movement.

Acknowledgements

We thank Diamond Light Source for access to beamline I03 (proposal mx17212) that resulted in the data presented here. S.M is supported by a post-graduate studentship from the Alzheimer's Society (UK) awarded to K.R.A. and V.S. [grant number - 286 (AS-PhD2015b-006)]. This research made use of the Balena High Performance Computing (HPC) Service at the University of Bath.

Author contributions

S.M performed all the experiments, analysed the data and wrote the manuscript. V.S. supervised the study and edited the manuscript. K.R.A. conceptualised and supervised the study, analysed the data and edited the manuscript.

Additional information

Accession code: The atomic coordinates and structure factors (code 6GID) have been deposited in the Protein Data Bank (http://www.pdb.org).

Competing financial interests

The authors declare no competing financial interests.

References

Adams, P.D., Afonine, P. V., Bunkóczi, G., Chen, V.B., Davis, I.W., Echols, N., Headd, J.J., Hung, L.-W., Kapral, G.J., Grosse-Kunstleve, R.W., McCoy, A.J., Moriarty, N.W.,

Oeffner, R., Read, R.J., Richardson, D.C., Richardson, J.S., Terwilliger, T.C., Zwart, P.H., 2010. Phenix: a comprehensive Python-based system for macromolecular structure solution. Acta Crystallogr. Sect. D Biol. Crystallogr. 66, 213–221.

Baker, N.A., Sept, D., Joseph, S., Holst, M.J., McCammon, J.A., 2001. Electrostatics of nanosystems: Application to microtubules and the ribosome. Proc. Natl. Acad. Sci. 98, 10037–10041.

Berman, H., Henrick, K., Nakamura, H., 2003. Announcing the worldwide Protein Data Bank. Nat. Struct. Mol. Biol. 10, 980.

Binkowski, T., Naghibzadeh, S., Liang, J., 2003. CASTp: Computed atlas of surface topography of proteins. Nucleic Acids Res. 31, 3352-3355.

Chen, V.B., Arendall, W.B., Headd, J.J., Keedy, D.A., Immormino, R.M., Kapral, G.J., Murray, L.W., Richardson, J.S., Richardson, D.C., 2010. MolProbity: all-atom structure validation for macromolecular crystallography. Acta Crystallogr. Sect. D Biol. Crystallogr. 66, 12–21.

Dion, N., Cohen, P., Crine, P., Boileau, G., 1997. Characterisation of neprilysin (EC 3.4.24.11) S2′ subsite. FEBS Lett. 411, 140–144.

Emsley, P., Lohkamp, B., Scott, W.G., Cowtan, K., 2010. Features and development of Coot. Acta Crystallogr. Sect. D Biol. Crystallogr. 66, 486–501.

English, A.C., Done, SH., Caves, S.L., Groom, R.C., Hubbard, E.R,. 1999. Locating interaction sites on proteins: the crystal structure of thermolysin soaked in 2% to 100% isopropanol. Proteins 37, 628–640.

Evans, P.R., Murshudov, G.N., 2013. How good are my data and what is the resolution? Acta Crystallogr. Sect. D Biol. Crystallogr. 69, 1204–1214.

Glossop, M.S., Bazin, R.J., Dack, K.N., Fox, D.N.A., MacDonald, G.A., Mills, M., Owen,

D.R., Phillips, C., Reeves, K.A., Ringer, T.J., Strang, R.S., Watson, C.A.L., 2011. Synthesis and evaluation of heteroarylalanine diacids as potent and selective neutral endopeptidase inhibitors. Bioorg. Med. Chem. Lett. 21, 3404–3406.

Hersh, L.B., Morihara, K., 1986. Comparison of the subsite specificity of the mammalian neutral endopeptidase 24.11 (Enkephalinase) to the bacterial neutral endopeptidase Thermolysin. J. Biol. Chem. 261, 6433–6437.

Howell, S., Nalbantoglu, J., Crine, P., 1995. Neutral endopeptidase can hydrolyze β-amyloid (1-40) but shows no effect on β-amyloid precursor protein metabolism. Peptides 16, 647–652.

Im, H., Manolopoulou, M., Malito, E., Shen, Y., Zhao, J., Neant-Fery, M., Sun, C.Y., Meredith, S.C., Sisodia, S.S., Leissring, M.A., 2007. Structure of substrate-free human insulin-degrading enzyme (IDE) and biophysical analysis of ATP-induced conformational switch of IDE. J. Biol. Chem. 282, 25453–25463.

Kerr, M.A., Kenny, A.J., 1974. The purification and specificity of a neutral endopeptidase from rabbit kidney brush border. Biochem. J. 137, 477–488.

Malito, E., Hulse, R.E., Tang, W.J., 2008. Amyloid-β degrading cryptidases: insulin degrading enzyme, presequence peptidase, and neprilysin. Cell. Mol. Life Sci. 65, 2574–2585.

McCord, L.A., Liang, W.G., Dowdell, E., Kalas, V., Hoey, R.J., Koide, A., Koide, S., Tang, W.-J., 2013. Conformational states and recognition of amyloidogenic peptides of human insulin-degrading enzyme. Proc. Natl. Acad. Sci. 110, 13827–13832.

McCoy, A.J., Grosse-Kunstleve, R.W., Adams, P.D., Winn, M.D., Storoni, L.C., Read, R.J., 2007. Phaser crystallographic software. J. Appl. Crystallogr. 40, 658–674.

McNicholas, S., Potterton, E., Wilson, K.S., Noble, M.E.M., Emsley, P., Murshudov, G.N., Cohen, S., Perrakis, A., Noble, M., 2011. Presenting your structures: the CCP4mg

molecular-graphics software. Acta Crystallogr. Sect. D Biol. Crystallogr. 67, 386–394.

Murshudov, G.N., Skubák, P., Lebedev, A.A., Pannu, N.S., Steiner, R.A., Nicholls, R.A., Winn, M.D., Long, F., Vagin, A.A., 2011. REFMAC5 for the refinement of macromolecular crystal structures. Acta Crystallogr. Sect. D Biol. Crystallogr. 67, 355–367.

Natesh R Schwager S.L., Sturrock, E.D., Acharya, K.R., 2003. Crystal structure of the human angiotensin-converting enzyme-lisinopril complex. Nature 421, 551–554.

Oefner, C., D'Arcy, A., Hennig, M., Winkler, F.K., Dale, G.E., 2000. Structure of human neutral endopeptidase (neprilysin) complexed with phosphoramidon. J. Mol. Biol. 296, 341–349.

Oefner, C., Pierau, S., Schulz, H., Dale, G.E., 2007. Structural studies of a bifunctional inhibitor of neprilysin and DPP-IV. Acta Crystallogr. Sect. D 63, 975–981.

Oefner, C., Roques, B.P., Fournie-Zaluski, M.C., Dale, G.E., 2004. Structural analysis of neprilysin with various specific and potent inhibitors. Acta Crystallogr. Sect. D 60, 392–396.

Sahli, S., Frank, B., Schweizer, W.B., Diederich, F., Blum- Kaelin, D., Aebi, J.D., Böhm, H., Oefner, C., Dale, G.E., 2005. Second- Generation Inhibitors for the Metalloprotease Neprilysin Based on Bicyclic Heteroaromatic Scaffolds: Synthesis, Biological Activity, and X- Ray Crystal- Structure Analysis. Helv. Chim. Acta 88, 731–750.

Schiering, N., D 'Arcy, A., Villard, F., Ramage, P., Logel, C., Cumin, F., Ksander, G.M., Wiesmann, C., Karki, R.G., Mogi, M., 2016. Structure of neprilysin in complex with the active metabolite of sacubitril Sci. Rep. 6, 27909. doi: 10.1038/srep27909.

Schrödinger, L., 2015. The PyMOL Molecular Graphics System, Version 1.8.

Sexton, T., Hitchcook, L.J., Rodgers, D.W., Bradley, L.H., Hersh, L.B., 2012. Active Site

Mutations Change the Cleavage Specificity of Neprilysin. PLoS One 7, 1–10.

Skidgel, R.A., Engelbrecht, S., Johnson, A.R., Erdös, E.G., 1984. Hydrolysis of substance P and neurotensin by converting enzyme and neutral endopeptidase. Peptides 5, 769–776.

Terwilliger, T.C., Grosse-Kunstleve, R.W., Afonine, P.V, Moriarty, N.W., Adams, P.D., Read, R.J., Zwart, P.H., Hung, L.W., 2008. Iterative-build OMIT maps: map improvement by iterative model building and refinement without model bias. Acta Crystallogr. Sect. D 64, 515-524

Tiraboschi, G., Jullian, N., Thery, V., Antonczak, S., Fournie-Zaluski, M.-C., Roques, B.P., 1999. A three-dimensional construction of the active site (region 507–749) of human neutral endopeptidase (EC.3.4.24.11). Protein Eng. Des. Sel. 12, 141–149.

Waterman, D.G., Winter, G., Gildea, R.J., Parkhurst, J.M., Brewster, A.S., Sauter, N.K., Evans, G., Sauter, K., Winter, G., Toyokawa, H., Wagner, A., 2016. Diffraction-geometry refinement in the DIALS framework. Acta Crystallogr. Sect. D Biol. Crystallogr. 39, 558–575.

Webster, C.I., Burrell, M., Olsson, L.-L., Fowler, S.B., Digby, S., Sandercock, A., Snijder, A., Tebbe, J., Haupts, U., Grudzinska, J., Jermutus, L., Andersson, C., 2014. Engineering neprilysin activity and specificity to create a novel therapeutic for Alzheimer's Disease. PLoS One 9, e104001.

Winn, M.D., Ballard, C.C., Cowtan, K.D., Dodson, E.J., Emsley, P., Evans, P.R., Keegan, R.M., Krissinel, E.B., Leslie, A.G.W., McCoy, A., McNicholas, S.J., Murshudov, G.N., Pannu, N.S., Potterton, E.A., Powell, H.R., Read, R.J., Vagin, A., Wilson, K.S., IUCr, 2011. Overview of the CCP4 suite and current developments. Acta Crystallogr. Sect. D Biol. Crystallogr. 67, 235–242.

Zheng, H., Cooper, D.R., Porebski, P.J., Shabalin, I.G., Handing, K.B., Minor, W., 2017.

CheckMyMetal: a macromolecular metal-binding validation tool. Acta Crystallogr. Sect. D 73, 223–233.

Table 1. Neprilysin X-ray data collection and refinement statistics.

Beamline	I03, DLS
Wavelength (Å)	0.976
Crystallographic statistics	
Space group	$P3_221$
Unit cell dimensions	
a,b,c (Å)	107.42, 107.42, 112.32
α, β, γ (◦)	90.00, 90.00, 120.00
Resolution range (Å)	93.03-1.90 (1.94-1.90)
R_{merge}	0.128 (1.384)
R_{meas}	0.130 (1.410)
$CC_{1/2}$	1.000 (0.665)
⟨ I/σ (I)⟩	25.3 (3.7)
Completeness (%)	100 (100)
No. observed reflections	3193442 (201035)
No. unique reflections	59422 (3790)
Multiplicity	53.7 (53.0)
Refinement	
R_{work} /R_{free} (%)	18.99/23.54
R.m.s deviations	
Bond lengths (Å)	0.009
Bond angles (◦)	0.894
Ramachandran statistics	
Favoured (%)	98
Allowed (%)	2
Outliers (%)	0
Wilson B-factor ($Å^2$)	30.8
Average B-factors ($Å^2$)	
Protein	34.0
Water	38.1
Zinc	24.9
Phosphate	37.1
Carbohydrate	54.5
No. of atoms	
Protein	5599
Water	463
Carbohydrate	56
PDB code	**6GID**

Values in parentheses are for highest-resolution shell.

Table 2. RMSD values from published inhibitor bound NEP structures superimposed onto the substrate-free structure. RMSD values were calculated in COOT using a least squares comparison for mainchain residues 54 – 749.

PDB code	RMSD	Reference
5JMY	0.426	Schiering *et al*., 2016
2YB9	0.354	Glossop *et al*., 2011
2QPJ	0.452	Oefner *et al*., 2007
1Y8J	0.421	Sahli *et al*., 2005
1R1H	0.385	Oefner *et al*., 2004
1R1I	0.484	Oefner *et al*., 2004
1R1J	0.421	Oefner *et al*., 2004
1DMT	0.340	Oefner *et al*., 2000

Figure legends

Figure 1. (A) SDS-PAGE of purified NEP sample. (B) Enzymatic assay for NEP measuring relative fluorescent units (RFU) over time. Fluorescent substrate Mca-RPPGFSAFK(Dnp) (10 μM), NEP (8 nM) and BSA (8 nM) were used. Each assay was conducted in triplicate and the average has been plotted with standard error bars.

Figure 2. Three-dimensional ribbon diagram of the NEP extracellular domain. The extracellular domain is further split into two subdomains coloured green for subdomain 1, red for subdomain 2 and cyan for the linker region. Observed glycan residues are displayed in purple and the zinc ion is displayed in grey.

Figure 3. NEP active site binding pocket labelled with subsites and residues

Figure 4. The active site zinc ion is coordinated by residues H583, H587, E646 and a phosphate ion. An additional PEG fragment is located in proximity to the phosphate ion. Electron density maps of the coordination sphere of the refined structure is shown. (A) 2mFo-DFc and (B) composite omit map. Both maps are shown to a contour level of 1.5σ.

Figure 5. Substrate-free NEP active site (green) is superimposed with 5JMY (Schiering *et al.,* 2016) (pink) (B) and 1DMT (Oefner *et al.,* 2000) (brick) (C). Inhibitors LBQ657 and phosphoramidon are shown in cyan and jade, with the zinc ion shown in grey.

Figure 6. Mainchain superpositions of substrate-free NEP with published structures: 5JMY (magenta), 2YB9 (light grey), 2QPJ (violet), 1Y8J (lime green), 1R1H (purple), 1R1I (grey), 1R1J (blue) and 1DMT (cyan).

Figure 7. (A) Molecular surface representation of front (left) and rear (right) of NEP and coloured green for subdomain 1, red for subdomain 2 and cyan for linker region. Small solvent entrances are indicated with an asterisk. (B) Molecular surface representation of front (left) and rear (right) for the central cavity of NEP. Electrostatic charge has been calculated with APBS. The electrostatic potential is measured in eV with scale bar indicated within the figure.

Figures

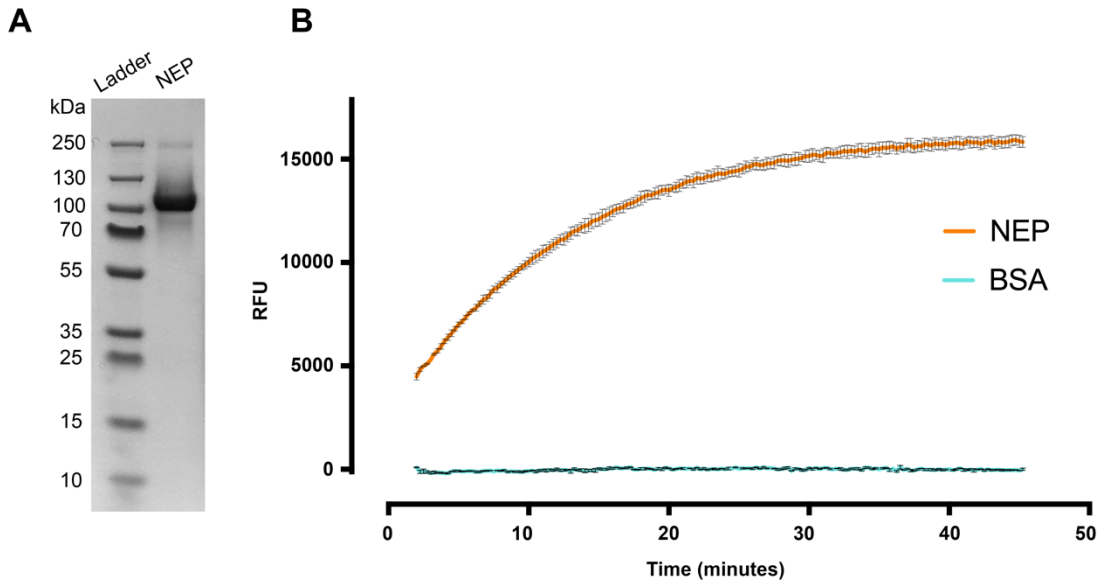

Figure 1.

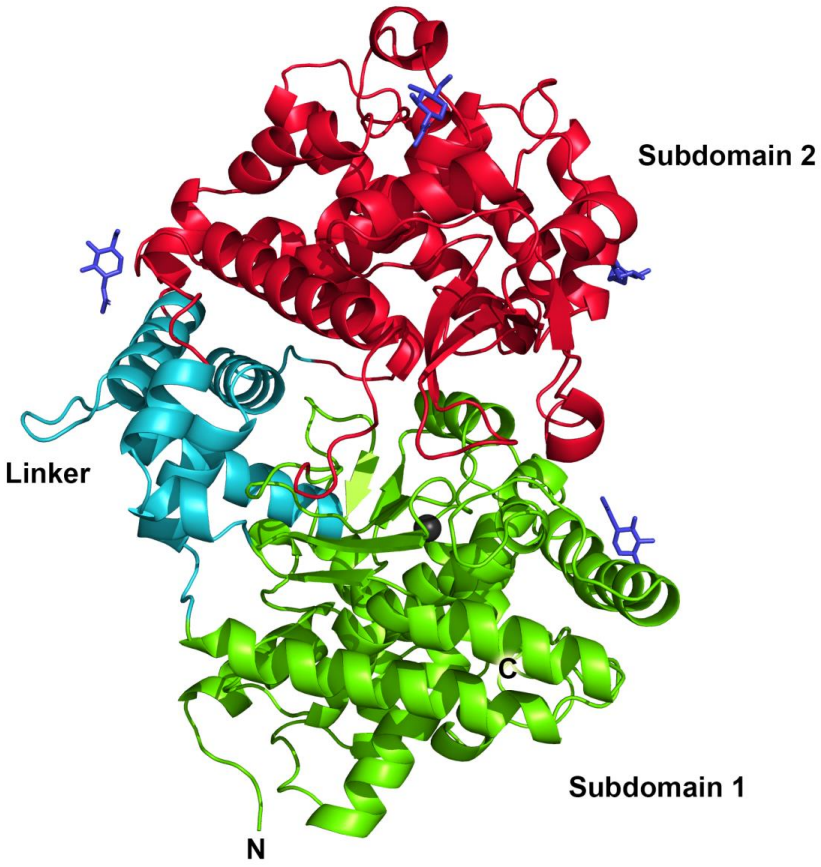

Figure 2.

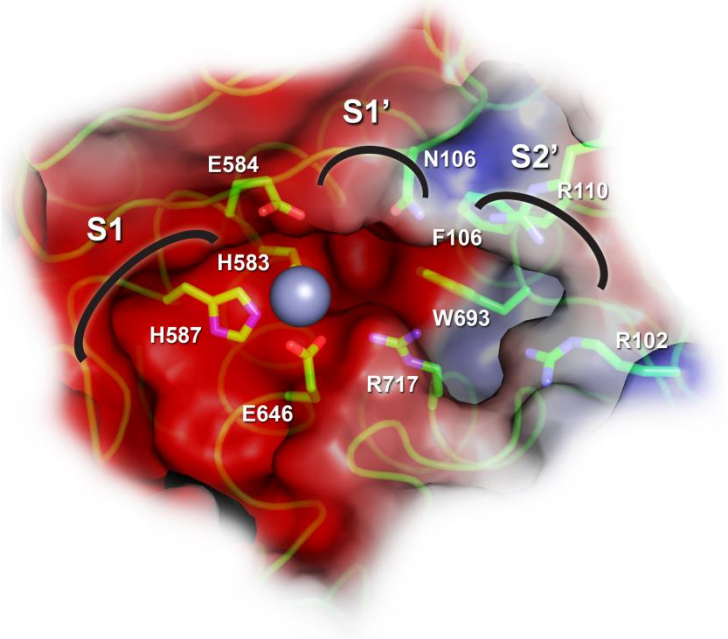

Figure 3.

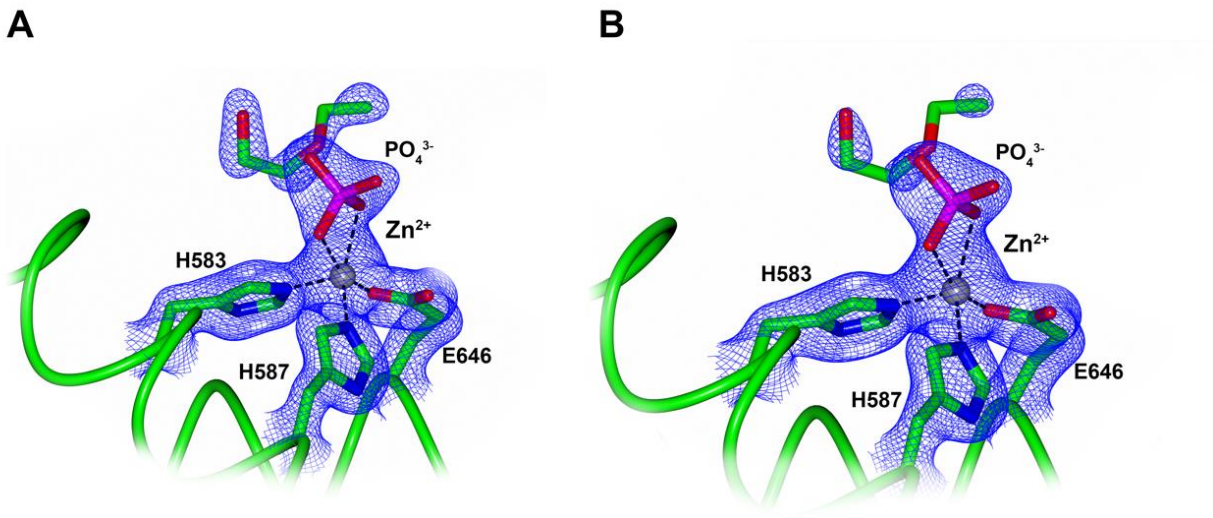

Figure 4.

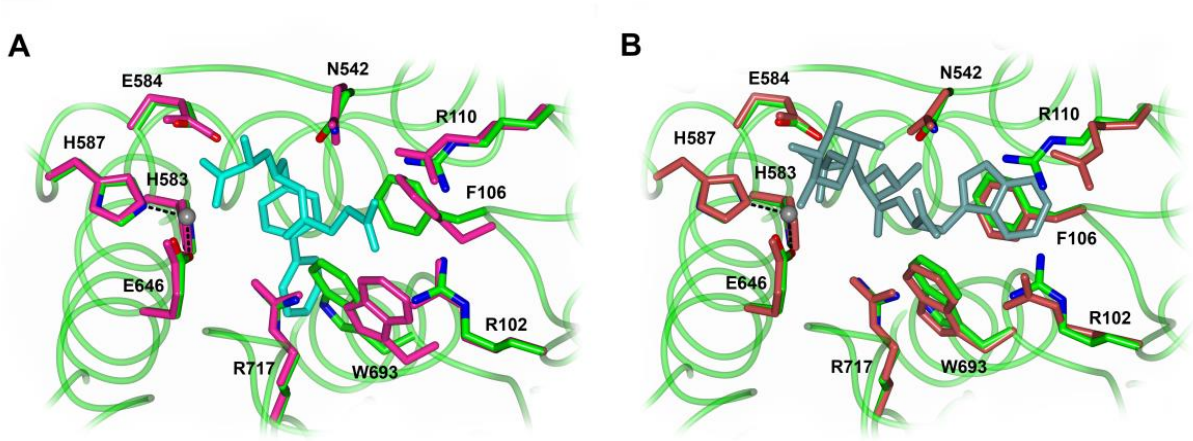

Figure 5.

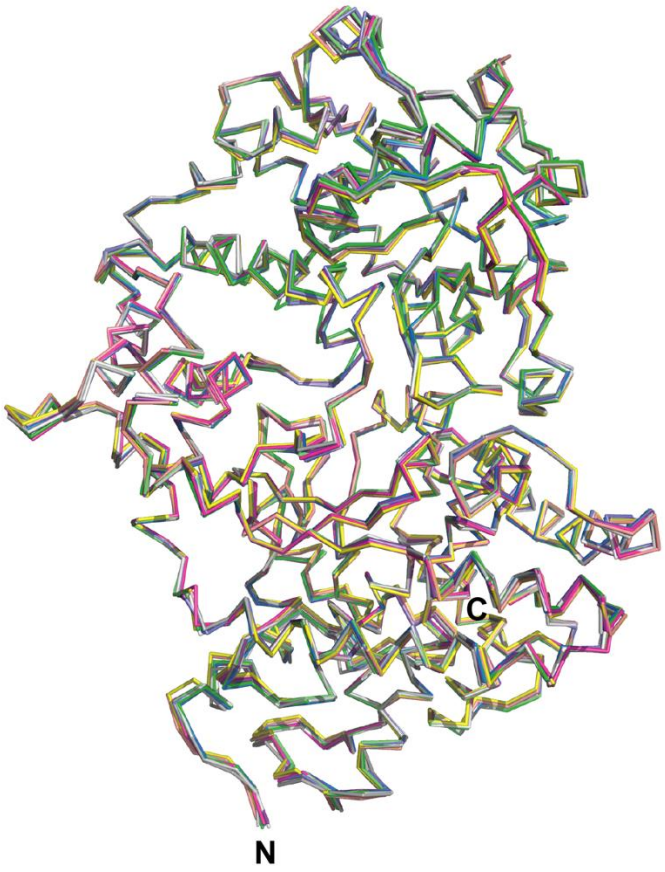

Figure 6.

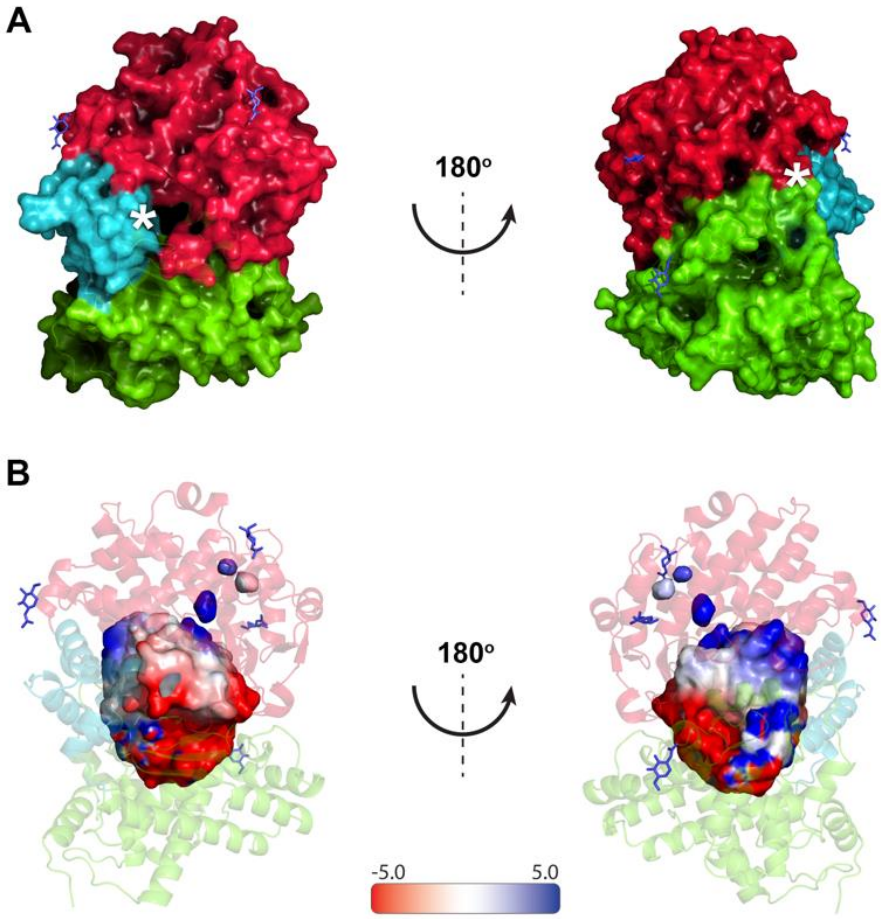

Figure 7.